January 1, 2000

Field-induced vacancy localization in a driven lattice gas: Scaling of steady states

M. Thies
Beate Schmittmann, *Iowa State University*

Field-induced vacancy localization in a driven lattice gas: Scaling of steady states

M. Thies[1,2] and B. Schmittmann[2]
[1]*Lehrstuhl WTM, Universität Erlangen–Nürnberg, Martensstrasse 5, 91058 Erlangen, Germany*
[2]*Center for Stochastic Processes in Science and Engineering and Department of Physics, Virginia Tech, Blacksburg, Virginia 24061-0435*
(Received 9 August 1999)

With the help of Monte Carlo simulations and a mean-field theory, we investigate the ordered steady-state structures resulting from the motion of a single vacancy on a periodic lattice which is filled with two species of oppositely ''charged'' particles. An external field biases particle-vacancy exchanges according to the particle's charge, subject to an excluded volume constraint. The steady state exhibits charge segregation, and the vacancy is localized at one of the two characteristic interfaces. Charge and hole density profiles, an appropriate order parameter, and the interfacial regions themselves exhibit characteristic scaling properties with system size and field strength. The lattice spacing is found to play a significant role within the mean-field theory.

PACS number(s): 05.40.−a, 68.35.Ct, 82.20.Mj

I. INTRODUCTION

Systems in nonequilibrium steady states have attracted considerable interest in the past decade [1]. While presenting a wealth of unexpected, intriguing phenomena, they are still quite poorly understood at a fundamental level. It is therefore natural to investigate simple model systems to identify generic behavior, before turning to real systems which are usually far more complex.

A particularly interesting class of model systems is based on lattice-gas models, involving one or several species of particles whose motion is biased in a specified direction. If the boundary conditions are open or periodic, the bias can drive the system out of a well-known equilibrium state into novel nonequilibrium steady states which typically carry global particle currents. Characteristic configurations, particle-particle correlations, and even phase transitions tend to be profoundly affected by the bias. Equilibrium phases can be suppressed, universality classes may change, and entirely new transitions can emerge. For example, in a simple driven Ising lattice gas with periodic boundary conditions [2], the bias suppresses one of the two ground states of the equilibrium system and fundamentally changes the universal properties of the Ising order-disorder transition [3–6]. In the high-temperature phase, it induces generic long-range correlations [7], which characterize all models of this type. Other anomalies are observed below T_c [8].

If the Ising symmetry is generalized [9,10] to include two (or more) species of particles which respond differently to the drive, such systems will generically exhibit blocking transitions, similar to traffic jams, in which one species impedes the motion of the other. These instabilities are genuine nonequilibrium transitions: they do not exist in the equilibrium limit and are controlled by particle density and bias strength, rather than temperature. The ordered phases exhibit characteristic spatial structures. Related real and model systems include water-in-oil microemulsions in external electric fields [11,12], gel electrophoresis [13], and traffic flow [14].

In this paper, we focus on a three-state lattice gas consisting of holes and two distinct species of particles driven by an external field E (the bias) in opposite directions [15]. We name the two species ''positive'' and ''negative,'' in analogy to charged particles in an electric field. The bias clearly breaks the Potts symmetry of the stochastic variable by acting differently on each species. The only interaction between the particles is an excluded volume constraint so that (i) each site can be occupied by at most one particle and (ii) particle-particle (''charge'') exchanges are not allowed. In the absence of other interparticle interactions, the temperature dependence of the system, reflecting a coupling to a heat bath, may be absorbed into the drive. Hence, the model is a high-field, high-temperature limit of a more complicated interacting system.

On a fully periodic square lattice, this system undergoes a blocking transition controlled by field strength and particle density, separating a homogeneous phase from a spatially inhomogeneous one [15]. For small mass density and drive, the steady-state configurations are disordered so that both particle densities are homogeneous and a significant charge current persists. In contrast, if a threshold mass density is exceeded, the particles form a single compact strip transverse to the field while the rest of the lattice remains essentially empty. The particle-rich region itself consists of two strips, also oriented transverse to the field, each dominated by one single species. In this phase, the particles impede one another, due to the excluded volume constraint, so that the charge current is much smaller. Other ordered phases, with nonzero winding number around the lattice (''barber poles''), are observed in systems with rectangular aspect ratios [16]. An analytical solution in the frame of a mean-field theory [15] was presented in Ref. [17]. With a slight geometrical modification, the model was also investigated by Foster and Godrèche [18].

Here, we focus on a novel aspect of the blocking transition, namely, a *localization phenomenon* occurring in systems near complete filling [19]. Thus, all lattice sites except a *single* vacant one are occupied by particles. For simplicity, we consider the symmetric situation, i.e., the particle numbers of each species differ at most by one. Starting from a disordered initial configuration, particles may exchange only with the vacancy. As a result, the hole diffuses through the lattice. However, it does *not* perform a Brownian random

walk, since the jump rate for a particle-hole exchange depends on the charge and direction of motion of the particle. By virtue of the bias, positive and negative particles are transported in opposite directions: The two particle species eventually segregate, provided the field exceeds a certain threshold, corresponding to the transition line [15]. When the steady state is reached, two strips have formed, filled by positive and negative particles, respectively. The hole itself ends up ''trapped'' on one of the two interfaces between the two ordered regions. Its location is the remnant of the empty region observed at finite hole density.

This problem, in both its static and dynamic aspects, is an example of a much wider ranging class of interacting random walk and defect-mediated domain-growth problems. The hole is a random walker whose motion changes its environment, but the environment reacts by determining the local jump rates. The vacancy plays the role of a highly mobile defect [20], interacting with an otherwise immobile background. The time evolution of the system, from an initially disordered particle background to two ordered strips, poses a domain-growth problem [21]. Clearly, a good understanding of the final *steady states* and their associated scaling properties is the first step in the analysis of the ordering process. This study forms the subject of this paper. We report elsewhere on the full *dynamics* [22].

The key results of our study [23] can be summarized as follows. First, we establish and confirm the characteristic scaling forms of the order parameter and the density profiles. Further, focusing only on the interfacial (as opposed to the fully ordered) regions of the profiles, we find that *both* interfaces are independent of the longitudinal system size and that their widths are controlled by the drive alone. These findings are reflected in our mean-field theory. Our results are limited in two ways: first, by the onset of the phase transition for small E, and second, by the breakdown of the naive continuum limit for large E.

This paper is organized as follows. In Sec. II, we give a precise definition of the microscopic model which underlies the Monte Carlo simulations. The relevant control and order parameters are defined. To set the scene, we provide a brief summary of earlier work. In particular, we discuss the blocking transition and its description in terms of a mean-field theory. In Sec. III, we investigate the scaling properties of the order parameter and the profiles, based on Monte Carlo simulations and the exact solution of the mean-field equations. We conclude with a summary and some comments.

II. THE MODEL: MICROSCOPICS AND MEAN-FIELD THEORY

In this section, we provide the necessary background. We begin with the microscopic definition of the model, followed by a summary of its phenomenology. We then provide a different perspective, by sketching the mean-field theory and its main results. We close with some technical details of the simulations.

Our model is defined on a two-dimensional square lattice of $L_x \times L_y$ sites with fully periodic boundary conditions. Each site, except one, can be occupied by a positive or negative particle. The remaining site is left empty. The resulting configurations can be described by an occupation variable $n^+_{x,y}$ ($n^-_{x,y}$), taking the value $+1$ if a positive (negative) charge is present at site (x,y) and zero otherwise. This enforces the excluded volume constraint. There are no other interactions between the particles. Turning to dynamics, particles may jump *only* onto the vacant site. In the absence of the external field, the vacancy exchanges randomly with any of its four nearest neighbors, independent of their charge and the direction of the move. This symmetry is broken by the ''electric'' field E, which is chosen to be uniform in space and time and directed along the positive y axis. For nonzero E, jumps transverse to the field are still random; however, parallel jumps are now biased: positive (negative) charges jump preferentially along (against) E. Specifically, the exchange rate of the hole with a randomly chosen nearest neighbor is given by the Metropolis rate [24],

$$W = \min\{1, \exp(qE\,\delta y)\}, \tag{1}$$

where $q = +1$ (-1) for a positive (negative) particle and $\delta y = 0, \pm a$ is the change of the y coordinate of the particle due to the jump. This choice mimics the local energetics of charges in a uniform field. The lattice constant a will be set to 1.

The dynamics of the model can be summarized by a master equation [25] for the probability $P(C,t)$ to find the system in the configuration $C = \{n^+_{xy}, n^-_{xy}\}$ at time t:

$$\frac{\partial}{\partial t} P(C,t) = \sum_{C'} \{W(C' \to C) P(C',t) - W(C \to C') P(C,t)\}. \tag{2}$$

Here, $W(C \to C')$ is the transition rate from C to C', specified by Eq. (1). For $E < \infty$, $P(C,t)$ approaches a unique steady-state solution $P^*(C)$ in the limit $t \to \infty$. For closed boundary conditions, $P^*(C)$ follows from equilibrium statistical mechanics, being the Boltzmann factor of a system of noninteracting charges in a uniform field. For periodic boundary conditions, however, there is no uniquely defined static potential for $E \neq 0$ so that $P^*(C)$ is not *a priori* known. Instead, it has to be found from an explicit solution of Eq. (1). Unfortunately, such solutions are available only for a few, mostly one-dimensional, cases. Here, we only know the $E = 0$ solution: the system is again in equilibrium, the particles diffuse randomly, and $P^*(C)$ is independent of configuration, i.e., $P^* \propto 1$.

The control parameters of this model are easily identified. In addition to the driving field E and the system size, $L_x \times L_y$, we can adjust the mass density

$$m \equiv \frac{1}{L_x L_y} \sum_{x,y} (n^+_{x,y} + n^-_{x,y}) \tag{3}$$

as well as the net charge density of the system:

$$\rho \equiv \frac{1}{L_x L_y} \sum_{x,y} (n^+_{x,y} - n^-_{x,y}). \tag{4}$$

Since the particle number of each species is separately conserved, both densities are also conserved. For our case, there is always a single hole, so that the particle density

$$m = 1 - \frac{1}{L_x L_y} \tag{5}$$

depends on the system size. Since we focus on nearly equal numbers of positive and negative particles, the net charge density is zero for systems with an odd number of sites and $-1/(L_x L_y)$ for an even number (the hole always takes the place of a positive particle). In the simulations, this small difference does not appear to lead to observable effects, unlike the case of $\rho = O(1)$ [26].

A brief description of the blocking transition and the associated phases will be helpful. For small values of drive and total mass, the system is in the disordered phase, characterized by spatially uniform mass and charge densities. A significant charge current flows in this phase. As E or m increase, a transition into an ordered phase, with spatially inhomogeneous densities, occurs. For systems with aspect ratios near unity, each species of particles forms a compact, stable strip transverse to the electric field. The strip of positive charges is located directly ''upfield'' from the negative strip, so that the strips block each other, due to the excluded volume constraint. The rest of the lattice remains essentially empty. Clearly, the current is much smaller in this phase. In the following, we will investigate the structure of these transverse strips when the empty region has shrunk to a single hole. We never observe strips with nonzero winding number: they appear to be suppressed near complete filling.

To distinguish ordered and disordered phases, a suitable order parameter is needed. It is convenient to introduce the local *hole* and *charge* densities:

$$\phi_{x,y} = 1 - (n^+_{x,y} + n^-_{x,y}) \quad \text{and} \quad \psi_{x,y} = n^+_{x,y} - n^-_{x,y}. \tag{6}$$

Since our system does not develop inhomogeneities in the x direction, it is natural to focus on the mass and charge-density *profiles*:

$$\phi(y) = \frac{1}{L_x} \sum_x \phi_{x,y} \quad \text{and} \quad \psi(y) = \frac{1}{L_x} \sum_x \psi_{x,y}. \tag{7}$$

Following Ref. [15], we define an order parameter

$$Q_L \equiv \frac{1}{m L_y} \left\langle \sum_y [\psi(y)]^2 \right\rangle. \tag{8}$$

The angular brackets denote a configurational average. Squaring the charge-density profile (which can have either sign) prevents unwanted cancellations in the sum over y. In the ordered phase, Q_L is $O(1)$, while being only order $O(1/(mL_x))$ in the disordered phase. Roughly speaking, $m L_y Q_L$ counts the ordered rows transverse to the external field. For a perfectly ordered system, Q_L would be unity. Clearly, other definitions of an order parameter are possible. In particular, the amplitude of the lowest Fourier component of either $\psi(y)$ or $\phi(y)$ is a much more sensitive measure for a study of the transition line [4,19]. Here, however, our focus is not on the transition but on the structure of ordered states, so that Q_L serves its purpose well.

Finally, let us add a comment on the transition line. Earlier simulation data [15] show that the threshold mass, m_c, depends strongly on E and the longitudinal system length L_y, but only weakly (if at all) on L_x. It can be first or second order [17,19], in different regions of parameter space. In our case, where only a single hole is present, the mass density is unity, to excellent accuracy. Therefore, the transition is controlled by E and L_y alone.

We now turn to a brief summary of the theoretical analysis [15,17] which will be essential for the following. Even though the master equation is just a linear equation, in practice it is not susceptible to theoretical analysis. To proceed, a continuum description is introduced, in the form of equations of motion for the *coarse-grained* hole- and charge-density profiles. Since the latter are both conserved quantities, the equations of motion take the form of continuity equations. They can be derived phenomenologically [15] or directly from the master equation [19]. In the latter case, we first write a set of equations for the local averages, $\langle \phi_{x,y} \rangle$ and $\langle \psi_{x,y} \rangle$, on discrete space (with lattice constant 1) and then take a *naive* continuum limit, e.g., we approximate $\langle \frac{1}{2}(\phi_{x+1,y} - \phi_{x-1,y}) \rangle$ by a first derivative with respect to x, etc. A mean-field assumption is necessary since two-point correlations must be truncated in order to obtain a closed set of equations. These can easily be written in general dimension d:

$$\partial_t \phi(\vec{r},t) = \vec{\nabla} \cdot \{ \vec{\nabla} \phi + \mathcal{E} \phi \psi \hat{y} \},$$
$$\partial_t \psi(\vec{r},t) = \vec{\nabla} \cdot \{ \phi \vec{\nabla} \psi - \psi \vec{\nabla} \phi - \mathcal{E} \phi (1 - \phi) \hat{y} \}. \tag{9}$$

Here, the hole density ϕ and the charge density ψ are functions of the d-dimensional coordinate $\vec{r}$ (with associated gradient $\vec{\nabla}$) and time t. The drive appears in these equations via its coarse-grained equivalent, the *effective* drive $\mathcal{E}$:

$$\mathcal{E}(E) = 2 \tanh(E/2), \tag{10}$$

pointing along the unit vector $\hat{y}$. A diffusion constant has been absorbed into the time scale. Derivatives higher than second order have been neglected, anticipating smoothly varying solutions. The equations have to be supplemented with periodic boundary conditions and the constraints on total mass and charge. For later reference, we also define the parameter

$$\epsilon \equiv \mathcal{E} L_y, \tag{11}$$

which will play the role of a scaling variable.

Time-independent solutions of these equations reflect stationary phases of the discrete model. The disordered phase corresponds to a homogeneous solution, which is stable with respect to small perturbations provided m does not exceed a threshold value m_H, given by

$$m_H = [1 + (2\pi/\epsilon)^2]/2. \tag{12}$$

The profiles in this phase are uniform. In our case, where the lattice is nearly completely filled, i.e., $m \lesssim 1$, we need $\epsilon \lesssim 2\pi$ in order to find a stable homogeneous steady state. For an electric field $E = 1.0$, this implies rather small system sizes ($L_y < 7$).

To find a steady-state solution which corresponds to a transverse strip, we seek solutions that are inhomogeneous in

the y coordinate only. Equations (9) can be integrated once, with integration constants being the hole and the charge currents. The former vanishes by symmetry at zero total charge. The latter, being nonzero in general, will be denoted by $j\mathcal{E}$. After expressing ψ in terms of ϕ,

$$\psi(y)=\frac{\phi'(y)}{\mathcal{E}\phi(y)}, \tag{13}$$

and rescaling the spatial variable to $z\equiv y/L_y$, we obtain an ordinary differential equation for the function $\chi\equiv 1/\phi$:

$$\chi''(z)/\epsilon^2=-j\chi^2(z)+\chi(z)-1. \tag{14}$$

To satisfy the boundary conditions, χ should be periodic with period 1. Writing χ in terms of a potential $(1/\epsilon^2)\chi''=-(d/d\chi)\,V(\chi)$, a further integration leads to $\chi'=\epsilon\sqrt{2(U-V)}$, where U is another integration constant. Unique solutions exist for $j<1/4$ and appropriate U. Introducing the three roots $\chi_1\leqslant\chi_-\leqslant\chi_+$, defined via $2[U-V(\chi)]=(2j/3)\,(\chi_+-\chi)(\chi-\chi_-)(\chi-\chi_1)$, the solution [17] can be written using Jacobian elliptic functions [27],

$$\chi(z)=\chi_+-(\chi_+-\chi_-)\mathrm{sn}^2[\,\epsilon z\sqrt{(j/6)\,(\chi_+-\chi_1)}\,], \tag{15}$$

in the interval $0\leqslant z\leqslant 1/2$. The other half of the interval, $1/2\leqslant z\leqslant 1$, is described by symmetry around the point $z=1/2$. Thus, the hole density takes its *minimum* at $\phi(0)=1/\chi_+$ and its maximum at $\phi(\frac{1}{2})=1/\chi_-$. The third root, χ_1, lies outside the physical domain. It is convenient to define the parameters p and R:

$$p\equiv(\chi_+-\chi_-)/(\chi_+-\chi_1), \tag{16}$$

$$R\equiv[4K(p)/\epsilon]^2. \tag{17}$$

Here, K stands for the complete elliptic integral [27] and is a function of p. Quantities of interest, such as the mass m or current j, can be expressed in terms of p and R:

$$1-4j=R^2\,(1-p+p^2), \tag{18}$$

$$1-m=\frac{[1-R^2(1-p+p^2)]\,\Pi(n|p)}{2(1+R+pR)\,K(p)}, \tag{19}$$

where $\Pi(n|p)$ is the complete elliptic integral of the third kind and $n\equiv 3pR/(1+R+pR)$. In principle, Eqs. (16) and (19) can be inverted to give the physical parameters m and ϵ in terms of R and p. In practice, it is easier to generate functions of interest, e.g., $j(\epsilon,m)$ or the order parameter $Q_L(\epsilon,m)$, parametrically in p, which is allowed to range from 0 to an upper limit $p_0(\epsilon)<1$ [17]. The upper limit p_0 is defined by the vanishing of the current, $j(\epsilon,p_0)=0$, and plays a particularly important role in the context of this study: According to Eq. (19), the mass density m tends to unity as p approaches its upper limit $p_0(\epsilon)$. Thus, only values of p near p_0 will be of interest here, since our focus is on nearly filled systems. This observation is used later for approximations.

The solution for $\chi(z)$ generates both hole and charge densities: $\phi=1/\chi(z)$ and $\psi=\chi'/(\epsilon\chi)$. These solutions describe the ordered phase, i.e., particle-rich strips transverse to the field. For *fixed* mass, they depend only on the parameter $\epsilon=\mathcal{E}L_y$ and the variable $z=y/L_y$; thus, these functions satisfy scaling in these variables. Moreover, the order parameter Q_L is a function of ϵ alone, since the spatial variable is integrated out. Here, however, we have to be rather more careful: since our system, irrespective of its size, will always contain only a single hole, the mass is inherently size-dependent. We will return to this issue in the next section.

Since it is cumbersome to work with Eq. (15) directly, its approximation for $\epsilon\gg 1$ is very useful [17]. The sn function can be replaced by a tanh function, and the argument simplifies,

$$\chi(z)\simeq\chi_+-(\chi_+-\chi_-)\tanh^2(\epsilon z/2). \tag{20}$$

As a result, a (weak) discontinuity appears in the first derivative of χ at the symmetry point $z=1/2$. This is unfortunate for our purposes, since $z=1/2$ is also the location of the maximum hole density. A different approximation, to be presented in the next section, resolves this difficulty. We note in passing that Eq. (20) takes the form of the soliton in the Korteweg–de Vries equation [28].

Clearly, one should not expect such a mean-field theory to provide a quantitatively correct description of the phase transition. However, it gives excellent *qualitative* insight into the instability and the phase diagram [17]. Moreover, since our interest here focuses on behavior *deeply* in the ordered phase, fluctuations do not play a significant role, and a mean-field theory should be very reliable. In fact, we will see that its main limitations do not arise from the neglect of correlations, but from taking a naive continuum limit.

We conclude this section with a few technical details of the simulations. The linear system sizes, L_x and L_y, range from 16 to 48, with E in the range 0.2–1.2. A characteristic parameter set is that of our ''reference system,'' which will appear in all scaling plots: $E=0.8$ and $L_x\times L_y=16\times 24$. Thus, the mass density differs from unity by at most 0.4%, so that $m=1$ is often an excellent approximation. The statistical error of the simulation results is of the order of 5% and thus much larger. All initial configurations are random. In one Monte Carlo step (MCS), a nearest neighbor of the vacancy is chosen at random and an exchange is attempted with the rates (1). Averages are computed from 100 independent samples for each choice of parameters. The approach to steady state is extremely slow [22] for larger system sizes and sets real-time limits on our simulations. For example, a system with 16×24 sites at $E=0.8$ requires approximately 5×10^7 MCSs to reach the steady state. If we increase L_y from 24 to 36, which is a factor of 1.5 in system size, the required number of MCSs increases by roughly a factor of 10.

While averaging, e.g., Q_L, is rather simple, by first measuring Q_L for each sample and then averaging these data, some effort is needed to compute *average* density *profiles* from the configurational data. Due to translational invariance, strips can be centered at any y, and a careless average would ''wash out'' any inhomogeneities. To avoid this, we first shift the ordered strips in the different samples in such a way that they match before we average. A natural choice would be to center all strips on, e.g., $y=0$, by normalizing the phase of the largest wavelength Fourier component of the

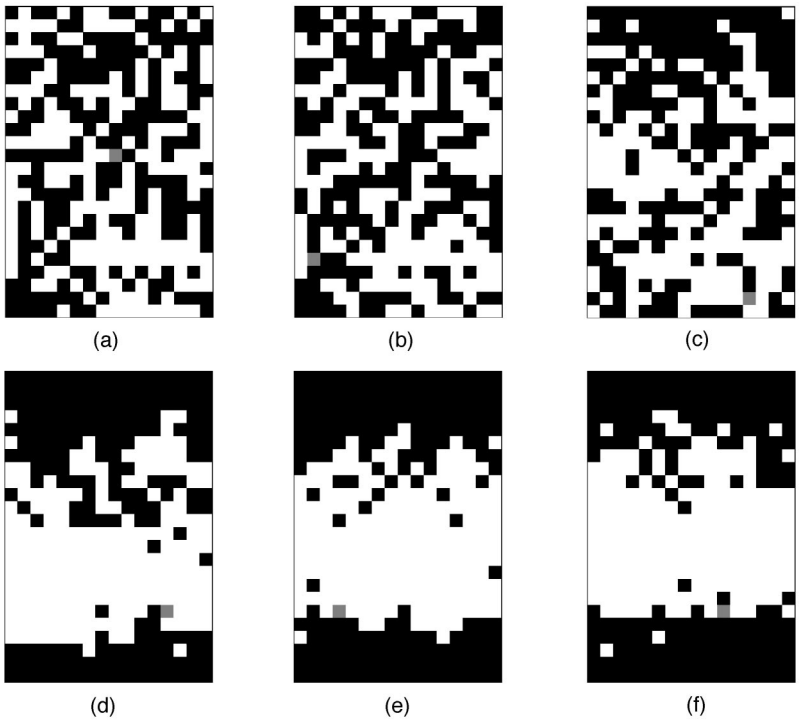

FIG. 1. Snapshots of an $L_x \times L_y$ system with $L_x = 16$ and $L_y = 24$ at $E = 0.8$, at different numbers of MCS: (a) 1, (b) 10^3, (c) 10^4, (d) 10^5, (e) 10^6, (f) 10^7. The initially disordered system undergoes a charge segregation. In the ordered steady-state configuration, the two oppositely charged particles are separated by two different interfaces. Minus particles are colored black, plus white, and the hole is gray. E field and y direction point upwards.

profile [19]. This is particularly useful when profiles are measured near the phase transition. Here, however, we will mostly take data deeply in the ordered phase, where the hole is essentially trapped. Thus, for each sample we keep track of the y position of the hole and determine the maximum of the hole density after a large number of MCSs. This maximum marks the interface between the positively and negatively dominated regions, the former located ''up-field'' from the latter. The charge-density profiles from different samples are now shifted such that these maxima coincide, and averages can be taken. Clearly, this procedure would run into difficulties if the interface were to wander significantly while the data for the hole-density profile are being accumulated. However, for the choices of the control parameters considered here, this does not appear to present major problems since fluctuations of the interface position are rather small. Moreover, they are very slow; thus, the time scales over which the interface remains well localized are sufficiently large to determine the maximum of the hole density very precisely.

III. SCALING BEHAVIOR IN THE STEADY STATE

As an introduction to the discussion of scaling properties, we illustrate the process by which the system approaches the steady state. A series of snapshots, taken at different MC times, first demonstrates why the dynamics is so slow, and second already suggests one of the key hypotheses of this work, namely, that the steady-state interfaces are well separated from one another. Figure 1 shows this series for our reference system. The negative (positive) particles are colored black (white) and the empty site is marked gray. A coordinate system is introduced in the usual way, i.e., the x direction lies horizontal, the y direction vertical, and the E field points upwards.

Starting from a random configuration [Fig. 1(a)], the system remains disordered for early times [Fig. 1(b)]. Eventually, by allowing positive (negative) particles to move preferentially upwards (downwards), the hole begins to segregate the two species. The early stages of this process are discernible in Fig. 1(c), where an interface between regions of opposite charge begins to develop. The position of this interface is determined by random fluctuations in the system. Clearly, due to the periodic boundary conditions, a second interface must also form. After 10^5 MCSs [Fig. 1(d)], the segregation of charges, and hence the two interfaces, are quite apparent. Due to the drive, the hole moves rapidly to the top (bottom) in regions of predominantly negative (positive) charge. Thus, it tends to remain near the interface which separates positive particles on the top from negative ones on the bottom [the lower interface in Figs. 1(d)–1(f)]. In contrast, it is rapidly driven away from the opposite interface. We will refer to the former (latter) interface as the ''downstream'' (''upstream'') one. The two interfaces are well separated, for this choice of parameters, and exhibit rather different morphologies: The downstream interface is quite sharp, while the upstream interface appears to be much more diffuse. To increase the degree of order in the system, the hole has to travel to the upstream interface before it can move another charge to a preferred position. Since this requires a series of *field-suppressed* jumps, the approach to the final steady state is very slow. As the ordered domain surrounding the downstream interface grows, the hole becomes strongly localized. A quantitative analysis of this ordering process will be provided elsewhere [22].

A picture of a typical steady-state configuration is shown in Fig. 1(f). To characterize these structures, we investigate three characteristic quantities: the order parameter Q_L, which provides a global measure of order, as well as the average hole- and charge-density profiles, which carry more detailed information about ordered configurations. All three of them are easily computed within the mean-field theory, as

we shall presently see. Since the spatial inhomogeneities form along the y direction, the system size L_x is not expected to play an important role. Simulations confirm this, provided the aspect ratio L_x/L_y does not exceed a certain threshold value, which is at least 6 in our case. For larger aspect ratios, strip configurations with nonzero winding number may begin to form, introducing an L_x dependence into the problem [16]. These, however, are not the subject of the present study.

A. The order parameter

We begin by calculating the order parameter Q_L in the mean-field approximation. Starting with the definition (8), we first express it within the continuum theory. Clearly, the summation over the sites in the y direction should be replaced by an integration. Using the rescaled variable $z=y/L_y$ and exploiting the symmetry of the profiles around $z=\frac{1}{2}$, we obtain

$$Q_L=\frac{2}{m}\int_0^{1/2}[\psi(z)]^2\,dz=\frac{2}{m\,\epsilon^2}\int_0^{1/2}\frac{\chi'^2}{\chi^2}\,dz. \tag{21}$$

In the last equality, we have recast ψ in terms of χ. To proceed, we change integration variable, from z to χ. The limits of the integral are transformed to $\chi(0)=\chi_+$ and $\chi(\frac{1}{2})=\chi_-$, where we recall that these are zeros of $U-V(\chi)$. With $\chi'=\sqrt{(2j\epsilon^2/3)\,(\chi_+-\chi)(\chi-\chi_-)(\chi-\chi_1)}$, we find

$$Q_L=\frac{4j}{3m}(Q_1+Q_2+Q_3+Q_4), \tag{22}$$

where we have introduced

$$Q_1=-\int_{\chi_-}^{\chi_+}\frac{\chi}{\chi'}d\chi, \tag{23}$$

$$Q_2=(\chi_1\chi_-\chi_+)\int_{\chi_-}^{\chi_+}\frac{1}{\chi^2\chi'}d\chi, \tag{24}$$

$$Q_3=(\chi_1+\chi_-+\chi_+)\int_{\chi_-}^{\chi_+}\frac{1}{\chi'}d\chi, \tag{25}$$

$$Q_4=-(\chi_+\chi_-+\chi_+\chi_1+\chi_-\chi_1)\int_{\chi_-}^{\chi_+}\frac{1}{\chi\chi'}d\chi. \tag{26}$$

The last two integrals are evaluated easily, giving 1/2 and $(1-m)/2$. The first two integrals can be reduced to complete elliptical integrals of the first, second, and third kind.

The resulting expressions can be expressed in more compact form, using the parameters m, p, and R [see Eqs. (16) and (17)]. For that purpose, it is helpful to write the three roots in terms of p and R:

$$\chi_1=\frac{2[1+R\,(p-2)]}{1-R^2\,(1-p+p^2)}, \tag{27}$$

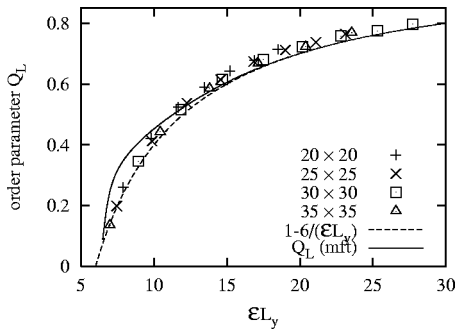

FIG. 2. Plot of order parameter vs $\epsilon=\mathcal{E}L_y$ for different square system square sizes ($20\leqslant L_x=L_y\leqslant 35$) and different electric fields ($0.2\leqslant E\leqslant 1.0$). The upper line shows the result of Q_L from mean-field theory, the lower line is its approximation $1-6/\epsilon$.

$$\chi_-=\frac{2[1+R\,(1-2p)]}{1-R^2\,(1-p+p^2)}, \tag{28}$$

$$\chi_+=\frac{2[1+R\,(1+p)]}{1-R^2\,(1-p+p^2)}. \tag{29}$$

Then, we invoke Eq. (18) to replace the current j and Eq. (19) to eliminate the elliptic integral of the third kind. Collecting, we obtain Q_L,

$$Q_L=1-\frac{1}{2m}\left\{R(p-2)+1+3R\frac{E(p)}{K(p)}\right\}. \tag{30}$$

E and K are the complete elliptical integrals of the first and second kind [27]. According to Eqs. (17) and (19), Q_L is a function of p and ϵ only, which can be generated parametrically in p.

So far, our discussion is valid for arbitrary mass m. Let us now consider the case of a single vacancy, namely $m=1-1/(L_xL_y)$, which corresponds to a system near complete filling. Considering only the leading terms in an expansion in powers of $\delta\equiv 1/(L_xL_y)$, the left-hand side of Eq. (19) is just δ. As a consequence, the factor $1-R^2(1-p+p^2)$ on the right-hand side is $O(\delta)$, and so is the current j, given by Eq. (18). Recalling that the upper limit p_0 of the p range is defined by the condition $j(\epsilon,p_0(\epsilon))=0$, we conclude that $p=p_0+O(\delta)$ for our case. Tracking the effect of the finite-size corrections through our preceding calculations, we find that χ_1, χ_+, and χ_- are all $O(L_xL_y)$, by virtue of their common denominator. To leading order, the hole density $\phi=1/\chi$ is therefore $O(\delta)$ as one might have anticipated. In contrast, the charge density is $O(1)$, due to Eq. (13). Since δ is very small in our study, all but the leading terms will be neglected in the following. Then, Q_L becomes a function of ϵ *alone*. This prediction is easily checked by Monte Carlo simulations.

In this spirit, we invoke Eq. (18) for $j=0$ and rewrite it as $\epsilon^2=[4K(p_0)]^2(1-p_0+p_0^2)$. Now, ϵ can be computed numerically for a set of discrete values of p in the interval [0,1]. The values of $Q_L(\epsilon,m=1)$, derived in this way, are shown as the solid theoretical curve in Fig. 2.

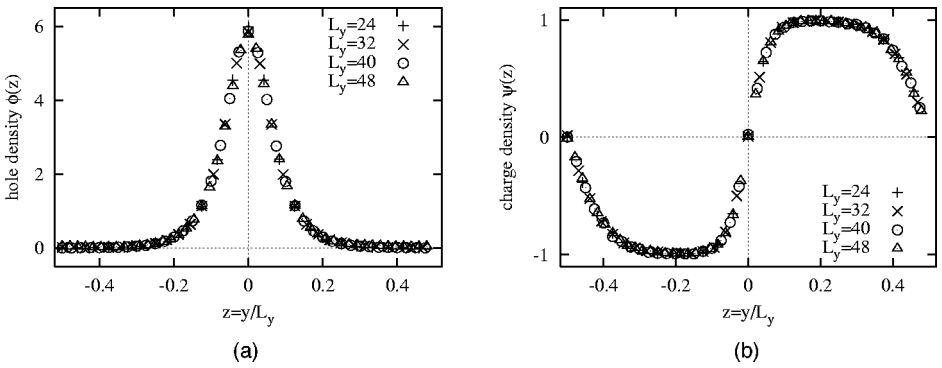

FIG. 3. Scaling plot of the hole (a) and charge (b) densities. L_y and E vary such that $\epsilon = 18.24$ remains constant. $L_x = 16$ is fixed.

For large $\epsilon \gg 1$, the approximations $R \simeq \sqrt{1-4j}$ and $p \simeq 1$ are valid. Within the same approximation, j can be replaced by $j = \exp(-m\epsilon/2)$ [17], which is vanishingly small. With $m = 1$, Q_L simplifies to

$$Q_L = 1 - \frac{6}{\epsilon}. \tag{31}$$

This gives rise to the dashed curve in Fig. 2. Comparing this approximation to the exact mean-field result, we see that both expressions are indistinguishable for $\epsilon > 18$. For smaller values of ϵ, the approximation underestimates the order parameter slightly.

Turning to simulation results, we first test the expected scaling in ϵ. Figure 2 shows data for the order parameter Q_L, for different square systems (ranging from 20×20 to 35×35) and different electric fields ($E = 0.2$–1.0), plotted versus ϵ. Each data point is an average over 30–50 samples. The size of the error bars is about 0.05 units. Within the accuracy of our data, all points lie on the same curve, corresponding to the scaling function. The latter appears to tend towards zero for $\epsilon \lesssim 6$. This is consistent with the stability limit of the inhomogeneous solutions, Eq. (12), which implies that for $m \approx 1$, an inhomogeneous solution can exist only if $\epsilon > 2\pi$. Once the transition to the homogeneous phase has occurred, the order parameter is of the order of $1/L_x \lesssim 0.05$. With increasing ϵ, the order parameter approaches its upper limit, i.e., 1.

It is remarkable, however, that the large ϵ approximation produces a better fit to the simulation data than the exact mean-field result, especially for $\epsilon < 10$. It is conceivable that the intrinsic errors of the mean-field theory approach are partially compensated by the large ϵ limit. Further studies are required to test this possibility. Focusing on the region $\epsilon > 15$, the simulation results all lie about 0.02 units above the theoretical curve. While these deviations are within the error bars of the data, they are too systematic to be ignored. Closer scrutiny reveals that the results of the large system sizes tend to be closer to the theoretical curves than those for small system sizes, which indicates that the differences between simulation and mean-field results are at least partly due to finite-size effects. We will return to this question at the end of Sec. III C.

B. Charge and hole density profiles

While the order parameter carries only global information about spatial inhomogeneities in the system, the charge- and hole-density profiles retain far more detail, allowing us to distinguish the oppositely charged domains and their interfaces. Based on the mean-field theory, we expect these densities to satisfy scaling in ϵ and z. This is borne out by the simulation results, which are presented in this section.

In order to exhibit the scaling of the densities, four different parameter sets (E, L_y) are simulated, generating 100 samples for each. The system length L_y and the electric field E are varied in such a way as to keep the parameter ϵ constant at 18.24. To avoid unwanted cancellations, we shift the maximum of the hole density in each run to $z = 0$ before averaging. The charge profiles are shifted accordingly. Thus, z covers the interval $(-0.5, 0.5)$, and the ''downstream'' interface is centered at the origin. In addition, we normalize the hole profile in such a way that all profiles enclose the same area.

A comment on this normalization is in order. Recalling the constraint on the total density, we have $1 - m = 1/(L_x L_y) = (1/L_y)\int_0^{L_y} \phi(y)\,dy$ for a single hole. Thus, we have $1 = L_x \int_0^{L_y} \phi(y)\,dy = L_x L_y \int_0^1 \phi(z)\,dz$ so that $L_x \phi(y)$ can be interpreted as the *probability density* for finding the hole in row y. Similarly, $L_x L_y \phi(z)$ is the probability density for finding the hole at position z. Thus, *normalized* plots for the hole density show the associated probability density, and the area under each curve is just 1. Moreover, since $\phi(z) = O[1/(L_x L_y)]$, according to the finite-size analysis in Sec. III A, the *normalized* quantity depends on z and ϵ alone. No such normalization is required for the charge density, since it is already of $O(1)$ in the system size.

To test for the anticipated scaling in ϵ and z, Monte Carlo data for the (normalized) hole density profile are presented in Fig. 3(a), and the charge-density profile is shown in Fig. 3(b). Since all data points collapse onto the same characteristic scaling curve for hole and charge profiles, respectively, the theoretical prediction is clearly confirmed.

Beyond demonstrating scaling, these plots provide a more quantitative characterization of the spatial structures in the system. Since ϵ here is the same as in Figs. 1(a)–1(f), Fig. 3(b) shows the associated steady-state charge-density profiles. We can see clearly that the particles are ordered in two regions, filling the whole system. Each of these regions consists essentially of one species. They are separated by two interfaces. The maximum of the hole density lies at the center $(z = 0)$ of the much sharper downstream interface where the field tends to localize the hole, while the minimum of the hole density marks the more diffuse upstream interface.

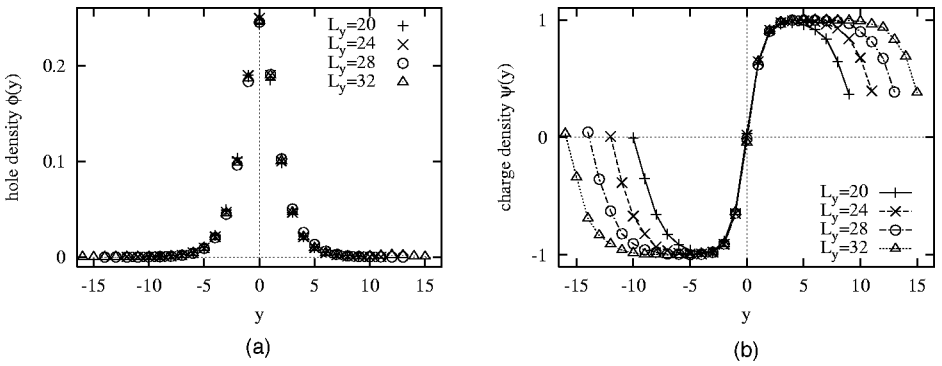

FIG. 4. Plot of the hole (a) and charge (b) densities for a range of L_y. $L_x=16$ and $E=0.8$ are constant.

To explore the size and field dependence of our system further, it is interesting to vary the system length L_y and the electric field E independently, *not* keeping ϵ constant. Of course, given the excellent data collapse of Figs. 3 and 4, we cannot expect global scaling over the whole y range. We will see, however, that certain *regions* of the profiles, centered on the two interfaces, still scale.

We first report simulations at constant electric field $E=0.8$ and transverse size $L_x=16$, increasing the longitudinal system size L_y from 20 to 32 in steps of 4. The (normalized) hole densities observed in these simulations are summarized in Fig. 4(a), plotted versus y rather than $z=y/L_y$.

We observe that the graphs associated with different L_y span different ranges of y, but are otherwise essentially indistinguishable in the central region. Thus, the width and the maximum of the hole density, and hence the width of the ''downstream'' interface, are not affected by changes in the longitudinal system size when plotted versus the y variable. We conclude therefore that the characteristics of this interface are controlled by the electric field alone (cf. the next section).

This behavior is also borne out by the charge-density profiles, Fig. 4(b). According to Eq. (13), the steady-state charge- and hole-density profiles are related via $\psi(y)=-\phi'(y)/[\mathcal{E}\phi(y)]$. Thus, the charge densities near the ''downstream'' interface should also be independent of L_y, in agreement with Fig. 4(b). On the other hand, the regions of nearly constant charge density must broaden to reflect the increasing system size. Thus, the profiles do not collapse at the edges of the plot. However, the similarity of their form near $y=\pm L_y/2$ suggests that the *upstream* interface might scale also, provided the profiles are shifted appropriately. This is indeed confirmed by the simulations [cf. Fig. 5(b) below]. Thus, the slopes and widths of the profiles, near *both* interfaces, are independent of system size. The remaining effect of L_y is very simple and can be observed in Fig. 4(b): Outside the interfacial regions, the charge densities saturate very rapidly at ± 1, and these saturated regions expand or contract to accommodate the selected system size.

It is now quite apparent how the profiles should scale if L_y remains fixed and E is varied instead. Since the interfacial regions are independent of L_y, but scale in z and ϵ, they must depend on y through the combination $\mathcal{E}y$. To check this conjecture, we fix the system size at $L_x\times L_y=16\times 24$, while the electric field increases from 0.4 to 1.2 in steps of 0.2. Figure 5(a) shows the (normalized) hole-density profile plotted versus the scaling variable $\mathcal{E}y$. The data collapse in the interfacial region is excellent, except for the smallest field $E=0.4$. This value of E, however, is rather close to the transition line where the mean-field theory is likely to break down. Focusing on the larger E's, it is apparent that the *width* of the downstream interface scales as $1/\mathcal{E}$. Turning to the charge densities, Eq. (13) implies that $\psi(y)$ is also a function of $\mathcal{E}y$ near the downstream interface. This is indeed confirmed by simulations. To illustrate the scaling of the *upstream* interface, we present Fig. 5(b): Here, all profiles have been shifted by $L_y/2$ in order to center the upstream interface at the origin. Clearly, this interface also scales in the variable $\mathcal{E}y$. For completeness, we note that the only profile that does not reach saturation is the one for the smallest E, since this value is quite close to the phase transition.

Let us summarize the key findings of the simulations. First, the data for each profile collapse onto a single, *global* scaling curve if plotted as a function of $z=y/L_y$ at constant ϵ. Moreover, focusing only on the interfacial (as opposed to the saturation) region, we find that *both* interfaces are independent of L_y and that their widths scale as $1/\mathcal{E}$, provided we are not too close to the transition to the homogeneous phase. In the next section, we will consider these findings in light of our mean-field theory.

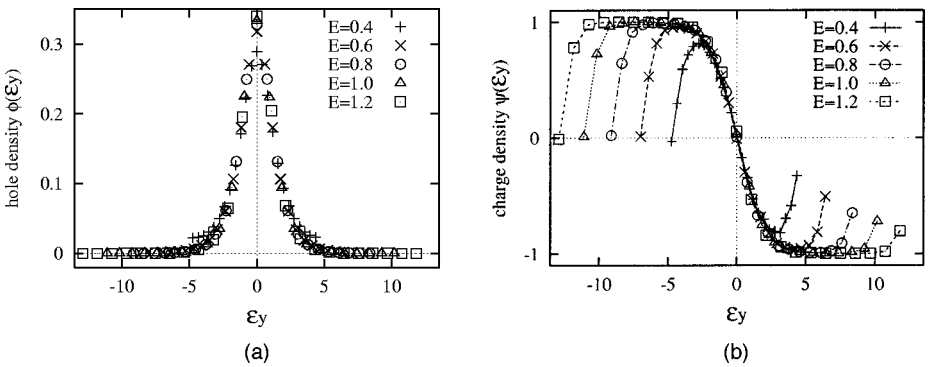

FIG. 5. Plot of the hole (a) and charge (b) densities for a range of E, vs $\mathcal{E}y$. $L_x=16$. Note that in (b) $y=0$ corresponds to the *minimum* of the hole density (upstream interface).

C. Independent interface approximation

In the following, we present an analytical description of the interfaces, which is then tested by detailed Monte Carlo simulations. We will focus in particular on the charge density since it directly determines the order parameter. First, we invoke the ''large ϵ'' approximation [17] to describe the upstream interface. A complementary approximation, involving a different version of the large ϵ limit, is then developed to describe the other (downstream) interface. The key assumption here is that the two interfaces are *independent* of one another, i.e., they are separated by sufficiently large ''saturation'' regions, which are entirely filled by either positive or negative charges, so that $\psi=\pm 1$ there. Such profiles result provided $\epsilon \gtrsim 18$, as demonstrated by Figs. 3(b), 4(b), and 5(b). The associated hole densities are approximately zero except near the downstream ($z=0$) interface [cf. Figs. 3(a), 4(a), and 5(a)].

Returning to the large ϵ limit of our mean-field theory, we recall that $\epsilon \gg 1$ is equivalent to $p \to 1$. In this limit, we may replace the Jacobian elliptic function sn by tanh [17]. In practice, this is already a good approximation for $\epsilon \geqslant 15$. It is easy to check that this results in (mean-field) profiles with vanishing hole densities near the upstream interface and saturated charge densities between the interfacial regions. Thus, this limit is consistent with our assumption of ''independent'' interfaces.

To describe the upstream interface, we start from Eq. (20) for large ϵ:

$$\chi(z)=\chi_+-(\chi_+-\chi_-)\tanh^2(\epsilon z/2). \tag{32}$$

Note that, due to the symmetry of χ, this equation holds for the interval $(-1/2,1/2)$. At $z=0$, χ takes its maximum, so that this is a good approximation for the upstream interface where $\phi=1/\chi$ is minimal. The largest deviation from the exact mean-field solution occurs at the boundaries, i.e., near the downstream interface, since this approximation violates the periodic boundary conditions: $\chi'(-1/2)\neq\chi'(1/2)$. The current is exponentially suppressed for large ϵ, i.e., $j \cong 6\, e^{-m\epsilon/2}$, and χ_+ and χ_- can be expressed in terms of j, namely, $\chi_+-\chi_- \cong 3/(2j)\sqrt{1-4j}$ and $\chi_+ \cong 1/(2j)(1+2\sqrt{1-4j})$ [17]. The hole and charge densities are now easily derived. In particular, recalling that $y=L_y z$, we can already read off the width ξ_u of the upstream interfacial region: $\xi_u=2L_y/\epsilon=2/\mathcal{E}$, which is consistent with the data. More specifically, we can compute the charge density from Eqs. (13) and (32). Neglecting terms of $O(j)$, we find

$$\psi(y)=-\tanh(\mathcal{E}y/2). \tag{33}$$

At the boundaries, Eq. (33) results in $\psi(\pm L_y/2)\to\mp 1$ in the large ϵ limit, which confirms that this approximation violates the boundary conditions. However, it does describe the interfacial region near $y=0$ very well. Rather than quoting the hole density explicitly, we only note that it is very small near the origin, namely $O(j)$.

In order to capture the downstream interface, we introduce another method. Since $j \cong 0$ to excellent accuracy for large ϵ [17], we return to the mean-field equations (9) and integrate them, setting *both* integration constants, i.e., hole *and* charge current, to zero. This is actually an equilibrium approximation, as we shall discuss below. The simulation data suggest the boundary conditions $\phi(\pm L_y/2)\simeq 0$ and $\psi(\pm L_y/2)\simeq\pm 1$. In this approximation, the downstream interface, corresponding to the *maximum* of the hole density, is localized at the origin. Written in terms of the variable y, Eq. (14) for χ simplifies to

$$\chi''(y)/\mathcal{E}^2=\chi(y)-1. \tag{34}$$

This is easily solved, subject to the specified boundary conditions:

$$\chi(y)=1+c\cosh(\mathcal{E}y). \tag{35}$$

To ensure that the hole density is strictly positive, we demand $c>0$. This constant can be determined explicitly from the mass constraint, namely $1=L_x\int_{-L_y/2}^{L_y/2}\phi(y)\,dy$, from which

$$2\frac{L_xL_y}{\epsilon\sqrt{c^2-1}}\arccos\left(\frac{1}{c}\right)=1 \tag{36}$$

in the large ϵ limit. In our simulations, L_x is at least 16 and $\mathcal{E}$ at most 2, so that $c>24$ follows. Thus, we can expand Eq. (36) for large c, resulting in

$$c\simeq\frac{L_xL_y}{\epsilon}\pi. \tag{37}$$

In fact, this approximation is already very good for $c>4$. Next, we compute the charge density,

$$\psi(y)=\frac{\sinh(\mathcal{E}y)}{\cosh(\mathcal{E}y)+c^{-1}}\simeq\tanh(\mathcal{E}y). \tag{38}$$

The last approximation is very accurate since $c>24$. Again, we can read off the width of the interfacial region, $\xi_d=1/\mathcal{E}$. Similar to the downstream interface, the width scales with $1/\mathcal{E}$, in agreement with the data. Intriguingly, however, our approximation is capable of reproducing the observation that the downstream interface is *narrower* than the upstream one. Whether the measured widths differ by a simple factor of 2, as predicted by our calculation, awaits a more quantitative comparison with Monte Carlo data.

In contrast to the upstream interface, ϕ is nontrivial here:

$$\phi(y)=\frac{1}{1+c\cosh(\mathcal{E}y)}\simeq\frac{1}{c\,\cosh(\mathcal{E}y)}, \tag{39}$$

confirming the width of the downstream interface $\xi_d=1/\mathcal{E}$. Away from the origin, the hole density again decays very rapidly, to match with its value near the upstream interface.

Before turning our focus on a comparison of these results with computer simulations, a last remark on the approximation of the downstream interface is in order. Imposing brick-wall (i.e., closed) rather than periodic boundary conditions, the approximation taken here (setting the current to zero) becomes exact. Moreover, the brick-wall system is an *equilibrium* one. The hole will accumulate positive (negative) charged particles at the top (bottom) of the system, thus establishing our boundary condition $\psi(\pm L_y/2)\to\pm 1$. Clearly,

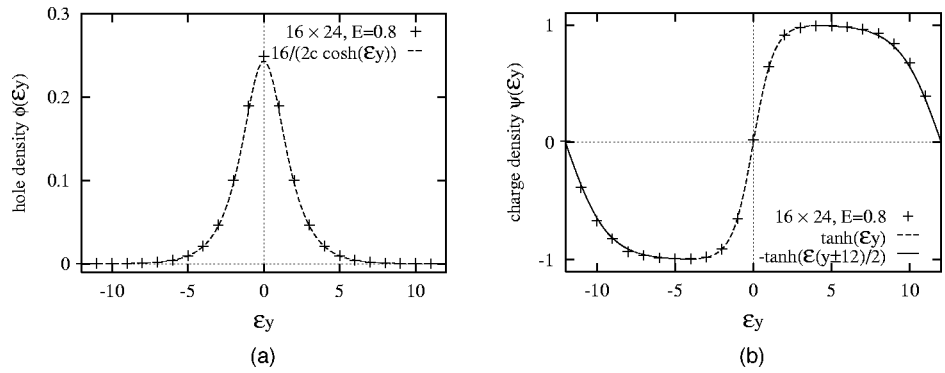

FIG. 6. (a) Plot of the hole density (+) for $L_x=16$, $L_y=24$, and $E=0.8$. The dashed line denotes the approximation Eq. (38), for the downstream interface, for $c=65.58$. Note that the hole density is vanishingly small near the upstream interface. (b) Plot of the charge density (+) for $L_x=16$, $L_y=24$, and $E=0.8$. The dashed and solid lines are the two interface approximations, Eqs. (33) and (38), matched at $y=\pm 4$.

only one nontrivial interface remains in this case, namely, the downstream one. In the steady state, the bias traps the hole near this interface. This fixes the boundary condition $\phi(\pm L_y/2)\to 0$. In this sense, our approximation for the downstream interface is equilibriumlike.

Returning to our model, we have obtained two compact equations (33) and (38) for the charge density. Since $\psi(y) \simeq \pm 1$ between the interfaces, to excellent accuracy, the whole system can be described in terms of the two interfaces, provided we match them appropriately. As an example, Fig. 6(b) shows a 16×24 system with $E=0.8$. The data points result from a Monte Carlo simulation while the solid and dashed lines reflect our two interface approximations, Eqs. (33) and (38), respectively. For the narrower interface (downstream, in the center), the match is nearly perfect, while for the wider interface (upstream, at the edges of the figure) the slope of the tanh function is slightly too small compared to the computer simulation. The agreement is nevertheless remarkable.

Next, we compare the approximation for the hole density with MC results. Here, we use Eq. (39) for the whole system since the hole density is vanishingly small except in the central region of the downstream interface. Simulation data and the analytic approximation for ϕ are presented in Fig. 6(a). A small quantitative discrepancy is observed at $y=0$, i.e., the center of the downstream interface, whereas all other data points are remarkably well reproduced by Eq. (39).

Given the results for the interfaces, we finally return to the order parameter Q_L. Here, we will see that the independent interface approximation provides us with a very intuitive picture for the approximate form (31). Since the steady state exhibits complete order in one region of positive and another one of negative particles, the deviation of Q_L from unity originates near the interfaces. We can easily compute the contribution to Q_L for each interface separately, using Eq. (21). The wider (upstream) interface reduces Q_L by $4/(\mathcal{E}L_y)$, while the narrower downstream interface lowers it by $2/(\mathcal{E}L_y)$, resulting in a net $Q_L=1-6/(\mathcal{E}L_y)$, in agreement with Eq. (31). Thus, this form simply tallies up the contributions of two well-separated interfaces, while the fully saturated regions give rise to the 1.

While these data for the scaling of order parameter and profiles are very convincing, the question of their range of validity must be raised. First, we should anticipate a breakdown of mean-field theory near the onset of the transition to the uniform state. This limits our analysis to $\epsilon \gtrsim 6$, corresponding to, e.g., $E\gtrsim 0.25$ for a system with $L_y=24$. For larger values of ϵ (but below an upper limit to be discussed shortly), scaling in ϵ and z is observed to hold. In order to have well-separated interfaces, we also require $\epsilon \gtrsim 15$. Beyond this threshold, the interfacial regions of the profiles scale very cleanly with $1/\mathcal{E}$.

In addition to a lower limit, there is also an upper limit for our analysis. Recalling Eq. (10), the effective drive is bounded: $\mathcal{E}\leqslant 2$, due to the tanh function, even for very large values of the microscopic E. Thus, within our mean-field theory, the interfacial widths cannot become arbitrarily small. For example, for the narrower downstream interface $\xi_d \leqslant 2$ in units of the lattice spacing, and $\psi(\pm 2)=\pm 0.96$, from Eq. (38). Thus, mean-field profiles require *at least* four lattice spacings to interpolate between the fully saturated regions. In contrast, *measured* charge-density profiles for large E (e.g., $E=2.0$) jump from -1 to $+1$ over just two lattice spacings. Such profiles are so sharp that our continuum limit fails to reproduce them: they can hardly be considered smoothly varying functions. As a result, the mean-field theory *underestimates* the order parameter for large values of E, which explains the systematic deviations of the smaller system sizes in Fig. 2. For example, $\epsilon=20$ in a 20×20 system corresponds to $E=1.2$, where this phenomenon is already noticeable. At a purely phenomenological level, we can extend the validity of our mean-field description if we retain the *form* of our equations (9) but replace the effective drive $\mathcal{E}$ by the microscopic field E everywhere. Mathematically, this requires keeping *explicit* track of the lattice constant a, followed by taking the *hydrodynamic* limit [29], i.e., $a\to 0$ at fixed drive, system size, and mass. Since the lattice constant appears in the rates, Eq. (1), the effective drive takes the form $\mathcal{E}=2\tanh(Ea/2)$. In the original discrete version of Eq. (9), the lattice constant appears in terms such as $\mathcal{E}\langle \frac{1}{2}(\phi_{x+a,y}-\phi_{x-a,y})\rangle$. In the limit of vanishing a, this expression simplifies to $Ea^2\partial\phi/\partial x$. Since the diffusive terms (e.g., $\nabla^2\phi$) also generate a factor a^2, the latter can be absorbed into the time scale so that we recover Eq. (9), with $\mathcal{E}$ replaced by E. Thus, all of our analytic results carry over, provided E takes the place of $\mathcal{E}$ everywhere [30]. With this

modification, the agreement of MC data and analytic description extends to the largest fields studied, namely, $E=2.0$.

To some extent, even the measured profiles do not reproduce the actual sharpness of the data fully. Since the downstream interface can form at an arbitrary location within the lattice, one should allow for *noninteger* shifts, i.e., shifts between 0 and 1 ($a=1$) modulo multiples of the lattice spacing, in order to produce accurate averaged data. This subtlety is not accounted for in our simulations, as seen from the discussion at the end of Sec. II. Thus, the actual interface is slightly smeared out when we average profiles by superposing the maxima of the hole density. Details can be found in Ref. [23]. To summarize briefly, our mean-field theory, in the form of Eqs. (9), gives excellent results provided $\epsilon \gtrsim 6$ and $E \leqslant 1.0$. If a systematic hydrodynamic limit is considered, the validity extends further, at least to $E \leqslant 2.0$.

IV. CONCLUSIONS

In this work, we focused on the scaling behavior of ordered steady states in a simple lattice model. A fully periodic lattice is filled with equal numbers of positive and negative ''charges,'' except a single site that remains empty. An external ''electric'' field, applied along one of the lattice axes, biases the motion of the particles. The dynamics is vacancy-mediated in that only vacancy-charge exchanges are allowed. The particles interact only through an excluded volume constraint.

This system develops spatial structures if EL_y, i.e., the product of drive and system size along the field direction, exceeds a critical value. Then, a charge-segregated strip, oriented transverse to the field, forms around the hole and grows until it fills the whole system. The two oppositely charged regions are separated by two interfaces with distinct characteristics: One interface, the ''downstream'' one, attracts the hole; the other (upstream) repels it strongly. This asymmetry finds its origin in the charge separation induced by the external field: while the hole moves rapidly *along* the field in the negative region, its preferred direction is reversed in the positive region.

Continuing earlier studies [15,17], we investigate the scaling properties of an appropriate order parameter and the hole and charge densities, as the external control parameters E and L_y vary. The transverse system size L_x plays no role except in finite-size corrections. Monte Carlo data are compared to the predictions of a mean-field theory in which the drive appears through the effective parameter $\mathcal{E} \equiv 2\tanh(E/2)$. The agreement is excellent, provided $\epsilon \equiv \mathcal{E}L_y \gtrsim 6$ so that we are in the ordered phase, and $E \leqslant 1.0$ to maintain fairly smooth profiles. The transverse system size L_x plays no role except in finite-size corrections. In particular, we can describe the charge-density profiles, with remarkable accuracy, in terms of two noninteracting interfaces, separated by perfectly ordered regions. The interfaces themselves are determined by the drive alone, independent of system size, and their widths scale with $1/\mathcal{E}$. For fields $E > 1.0$, the data show very steep slopes in the interfacial regions, which cannot be captured correctly by a naive continuum limit. Remarkably, the mismatch between data and mean-field theory is significantly reduced if we substitute the *microscopic* field E for the *effective* $\mathcal{E}$ in the (mean-field) interface approximations. The emergence of the latter can be understood in the limit of vanishing lattice constant. We should caution, however, that this limit must also eventually break down since it does not commute with the limit $E \to \infty$. Since the details of the continuum limit appear to play a key role here, it would be interesting to analyze the *discrete* precursor of Eq. (9). In this case, the natural parameter should be $\mathcal{E}$ alone.

Another interesting question concerns the character of the interfaces when a finite density of vacancies is present. In this case, the downstream interface ''splits'' into two halves, separated by an empty region. Clearly, in addition to E and L_y, the overall mass m now enters the criterion for having independent interfaces. Provided the appropriate condition is met, however, we expect that the interfacial profiles still depend only on $\mathcal{E}$: *local* structures appear to be controlled entirely by the drive.

Finally, our study paves the way for the exploration of dynamic phenomena in driven two-species models. Having established the scaling properties of the *final* steady states, work is in progress to investigate how they *develop* from random initial conditions [22].

ACKNOWLEDGMENTS

We wish to thank R. K. P. Zia, G. Korniss, and Z. Toroczkai for valuable discussions. Support from the National Science Foundation through the Division of Materials Research is gratefully acknowledged.

[1] B. Schmittmann and R.K.P. Zia, *Phase Transition and Critical Phenomena*, edited by C. Domb and J.L. Lebowitz (Academic, New York, 1995), Vol. 17.

[2] S. Katz, J.L. Lebowitz, and H. Spohn, Phys. Rev. B **28**, 1655 (1983); J. Stat. Phys. **34**, 497 (1984).

[3] H.K. Janssen and B. Schmittmann, Z. Phys. B: Condens. Matter **64**, 503 (1986); K.-t. Leung and J.L. Cardy, J. Stat. Phys. **44**, 567 (1986); **45**, 1087 (E) (1986) (Erratum).

[4] K.-t. Leung, Phys. Rev. Lett. **66**, 453 (1991); Int. J. Mod. Phys. C **3**, 367 (1992); J.-S. Wang, J. Stat. Phys. **82**, 1409 (1996); K.-t. Leung and J.-S. Wang, e-print cond-mat/9805285 (1998).

[5] B. Schmittmann and R.K.P. Zia, Phys. Rev. Lett. **66**, 357 (1991); B. Schmittmann, Europhys. Lett. **24**, 109 (1993).

[6] E. Praestgaard, H. Larsen, and R.K.P. Zia, Europhys. Lett. **25**, 447 (1994).

[7] M.Q. Zhang, J.-S. Wang, J.L. Lebowitz, and J.L. Valles, J. Stat. Phys. **52**, 1461 (1988); P.L. Garrido, J.L. Lebowitz, C. Maes, and H. Spohn, Phys. Rev. A **42**, 1954 (1990); G. Grinstein, D.H. Lee, and S. Sachdev, Phys. Rev. Lett. **64**, 1927 (1990); R.K.P. Zia, K. Hwang, B. Schmittmann, and K.-t. Leung, Physica A **194**, 183 (1993).

[8] K.-t. Leung, K.K. Mon, J.L. Valles, and R.K.P. Zia, Phys. Rev. Lett. **61**, 1744 (1988); K.-t. Leung, K.K. Mon, J.L. Valles, and R.K.P. Zia, Phys. Rev. B **39**, 9312 (1989); J.L. Valles, K.-t. Leung, and R.K.P. Zia, J. Stat. Phys. **56**, 43 (1989); K.-t. Leung, and R.K.P. Zia, J. Phys. A **24**, 1399 (1991); **26**, L737 (1993);

F.J. Alexander, C.A. Laberge, J.L. Lebowitz, and R.K.P. Zia, J. Stat. Phys. **82**, 1133 (1996); M. Anderson, Ph.D. thesis, Virginia Tech, 1998.

[9] R.B. Potts, Proc. Cambridge Philos. Soc. **48**, 106 (1952); F.Y. Wu, Rev. Mod. Phys. **54**, 235 (1982).

[10] M. Blume, V.J. Emery, and R.B. Griffiths, Phys. Rev. A **4**, 1071 (1971).

[11] See, e.g., S. Chandra, *Superionic Solids. Principles and Applications* (North-Holland, Amsterdam, 1981).

[12] M. Aertsens and J. Naudts, J. Stat. Phys. **62**, 609 (1990).

[13] M. Rubinstein, Phys. Rev. Lett. **59**, 1946 (1987); T.A.J. Duke, *ibid.* **62**, 2877 (1989); Y. Shnidman, *Mathematical and Industrial Problems IV*, edited by A. Friedman (Springer, Berlin, 1991); B. Widom, J.L. Viovy, and A.D. Desfontaines, J. Phys. I **1**, 1759 (1991).

[14] O. Biham, A.A. Middleton, and D. Levine, Phys. Rev. A **46**, R6124 (1992); K-t. Leung, Phys. Rev. Lett. **73**, 2386 (1994); J.M. Molera, F.C. Martinez, and J.A. Cuesta, Phys. Rev. E **51**, 175 (1995).

[15] B. Schmittmann, K. Hwang, and R.K.P. Zia, Europhys. Lett. **19**, 19 (1992).

[16] K.E. Bassler, B. Schmittmann, and R.K.P. Zia, Europhys. Lett. **24**, 115 (1993).

[17] I. Vilfan, B. Schmittmann, and R.K.P. Zia, Phys. Rev. Lett. **73**, 2071 (1994).

[18] D.P. Foster and C. Godréche, J. Stat. Phys. **76**, 1129 (1994).

[19] G. Korniss, B. Schmittmann, and R.K.P. Zia, Europhys. Lett. **32**, 49 (1995); J. Stat. Phys. **86**, 721 (1997); G. Korniss, Ph.D. thesis, http://scholar.lib.vt.edu/theses/available/etd-5637112239721111/ (Virginia Tech, 1997).

[20] See, e.g., W.D. Callister, Jr., *Materials Science and Engineering: An Introduction* (Wiley, New York, 1994); Z. Toroczkai, G. Korniss, B. Schmittmann, and R.K.P. Zia, Europhys. Lett. **40**, 281 (1997).

[21] J.S. Langer, *Solids Far From Equilibrium*, edited by C. Godrèche (Cambridge University Press, Cambridge, 1992); A. Bray, Adv. Phys. **43**, 357 (1994).

[22] B. Schmittmann and M. Thies (unpublished); M. Thies, Diplomarbeit, Technische Universität Braunschweig, 1999 (unpublished).

[23] M. Thies, Master's thesis, http://scholar.lib.vt.edu/theses/available/etd-81198-19472/ (Virginia Tech, 1998).

[24] N. Metropolis, A.W. Rosenbluth, M.N. Rosenbluth, A.H. Teller, and E. Teller, J. Chem. Phys. **21**, 1087 (1953).

[25] See, e.g., K. Binder, *Applications of the Monte Carlo Method in Statistical Physics* (Springer-Verlag, Berlin, 1983).

[26] K.-t. Leung and R.K.P. Zia, Phys. Rev. E **56**, 308 (1997). Here, a correlation-induced term is added to the mean-field equations. It is extremely small for our system.

[27] Notation from *Handbook of Mathematical Functions*, edited by M. Abramowitz and I.A. Stegun (Dover, New York, 1970), Chaps. 16 and 17.

[28] See, e.g., P.G. Drazin and R.S. Johnson, *Solitons: An Introduction* (Cambridge University Press, Cambridge, 1989).

[29] See, e.g., H. Spohn, *Large Scale Dynamics of Interacting Particles* (Springer-Verlag, Berlin, 1991).

[30] In the equilibrium approximation for the downstream interfacial region, the microscopic drive E emerges quite naturally. If we neglect the vacancy, we can use the Fermi-Dirac distribution to compute the configurational energy of the ''charges'' in an ''electric'' field E. The average occupation number of a given site can then be translated into a charge density profile. Reexpressing the chemical potential in terms of the total number of particles, as usual, we find $\psi(y)=\tanh(Ey)$, for the downstream interface [G. Korniss and B. Schmittmann (unpublished)].